Table 2. List of Name Abbreviations and Description of the Genes Analyzed in this Study

Gene Name	Description
Abl1	Mouse c-abl gene exon 1 of type II
Ccna1	Mouse mRNA for cyclin A1
Ccna2	Mouse mRNA for cyclin A2
Ccnb2	Mouse mRNA for cyclin B2
Ccne1	Mouse mRNA for cyclin E
Crkol	Mouse mRNA for Crkl protein
Csf1r	Mouse c-fms proto-oncogene
E2f5	Mouse mRNA for E2F-5 protein
Egfr	Mouse (BALB/c) Epidermal Growth Factor Receptor mRNA
Elk1	Mouse mRNA for elk1 protein
Elk4	Mouse sap1A mRNA
Ets1	Mouse ets-1 mRNA
Etv6	Mouse mRNA for TEL protein
Fgf3	Mouse int-2 gene
Figf	Mouse mRNA for new member of PDGF/VEGT family of growth factors
Fos	Mouse c-fos oncogene
Fosb	Mouse fosB mRNA
Il1a	Mouse mRNA for interleukin-1
Lmyc1	Mouse L-myc gene
Mybl2	Mouse B-myb mRNA
Myc	Mouse normal c-myc gene
Nmyc1	Mouse N-myc gene
Nras	Mouse mRNA for N-ras protein (exons 1 - 6 part.)
Pdgfb	Mouse platelet-derived growth factor B chain (c-sis) gene
Pgf	Mouse mRNA for placenta growth factor
Ptn	Mouse mRNA for OSF-1
Ret	Mouse mRNA for ret proto-oncogene
Tfdp1	Mouse mRNA for DRTF-polypeptide-1 (DP-1)
Tgfb2	Mouse mRNA for transforming growth factor-beta2
Thra	Mouse c-erbA-alpha mRNA for thyroid hormone receptor
Tlm	Mouse tlm oncogene for tlm protein
Cdkn2a	Mouse CDK4 and CDK6 inhibitor protein (p16ink4a)
Cdkn2d	Mouse p19 protein mRNA, complete cds
E2F1	Mouse E2F1 mRNA, complete cds
p53	Mouse mRNA for cellular tumour antigen p53
mdm2	Mouse mdm2 mRNA for mdm2 protein
Cdk7	Mouse mRNA for protein kinase crk4
Rbl1	Mouse p107 (p107) mRNA, complete cds
Rbl2	Mouse retinoblastoma-related protein Rb2/p130

fold-change data from the gene-expression data sets. This method falls under the general area of Bayesian networks, with a likelihood-based selection algorithm used to identify the most promising networks. In general, if $\boldsymbol{X_1}$, $\boldsymbol{X_2}$....$\boldsymbol{X_p}$ represents the data obtained for p genes, N denotes a network, and θ denotes parameters in that network, with the likelihood given by:

$$f_{X|N,\theta}(X_1,X_2,...,X_p \mid N,\theta)=\prod_{j=1}^{p} f_{X_j|N,\theta_j}(X_j \mid pa(X_j),N,\theta_j) \quad (1)$$

A. The choice of the best network would be the one with the largest value of the posterior density at the chosen network topology; that is

$$\text{find } \hat{N}=\arg\max_{N} f_{N|D}(N \mid D) \quad (2)$$

$$\text{where } f_{N|D}(N \mid D) \propto f_N(N)\cdot f_{D|N}(D \mid N) \quad (3)$$

B. The Bayesian network used in this analysis had the following assumptions:

$$\text{i) } f_N(N) \Rightarrow \text{ uniform distribution} \quad (4)$$

$$\text{ii) } f_{D|\theta,N}(D \mid \theta,N)=\prod_{j=1}^{p}\left\{\prod_{i=1}^{n} f_{X_j|N,\theta_j}(X_{ji} \mid pa(X_{ji}),N,\theta_j)\right\} \quad (5)$$

$$\text{iii) } f_{\theta|N}(\theta \mid N)=\prod_{j=1}^{p} f_{\theta_j|N}(\theta_j \mid N) \quad (6)$$

where pa (X_{ji}) is the collection of genes that link to the j^{th} gene in the network (a pathway).

with these assumptions,

$$\log f_{N|D}(N \mid D) \propto \sum_{j=1}^{p} \log \int \left\{\prod_{i=1}^{n} f_{X_j|N,\theta_j}(X_{ji} \mid pa(X_{ji}),N,\theta_j)\right\}\cdot f(\theta_j \mid N)\,d\theta_j \quad (7)$$

Thus, it is possible to focus on each gene rather than the whole network and still obtain a global optimum. To quantify rates in the gene-expression network, we used the Bayesian methods developed by Toyoshiba *et al.* [22, 23]. Supposing that $\boldsymbol{X_i}$ (i=*1,2,3...p*) represents the natural log of the relative ratio, the functional relationships between the genes could be characterized using the log-linear model below:

$$E(X_i \mid Pa(X_i),\beta_{i\bullet})=e^{\sum_{j=1}^{p} I_{ji}\beta_{ji}X_j} \quad (8)$$

where I_{ji} is an indicator function (-1, 0, 1) characterizing the effect from $\boldsymbol{G_j}$ to $\boldsymbol{G_i}$, T represents a matrix having I_{ij} as the (i,j) element, and $\beta_{i\cdot}=[\beta_{j1}, \beta_{j2}\beta_{j3}\beta_{j4}...\beta_{jp}]$ is the vector in which each β_{ji} is the magnitude by which one unit of gene $\boldsymbol{X_j}$ will affect the expression levels of gene $\boldsymbol{X_i}$. Thus, if *Iji* is not equal to 0, ***Pa(Xi)*** contains $\boldsymbol{X_j}$.

If $f(\boldsymbol{X_i} \mid T, \theta)$ is defined as the distribution of gene expression in the given model, then the likelihood is written as

$$f_{X|T,\theta}(X_1,X_2,.....X_P \mid T,\theta)=\prod_{j=1}^{p} f_{X_j|T,Pa(X_j),\theta}(X_j \mid T,Pa(X_j),\theta), \quad (9)$$

where θ represents the parameter vector in the model.

By Bayes' theorem, the prior distribution is given by

$$f_{\theta|X,T}(\theta \mid X,T) \sim f_{X|T,\theta}(X_1, X_2, ...X_p|T,\theta) \cdot f_\theta(\theta) \quad (10)$$

The posterior distributions $f_{\theta|X,T}$ were evaluated using the MCMC method. In our analyses, $f_{X|T,\theta}$ was assumed to be normal, with a mean defined by equation (8) and a random variance whose prior distribution was assumed to be uniform with 0 as the lower bound and twice the maximum STD for each gene distribution. The prior distribution for θ and f_θ was assumed to be lognormal with a mean of 0 and a variance of 1.0

The MCMC analysis was applied as described in [23] and [22]. A typical MCMC run was 100,000 samples with the first 20% of the samples discarded to "burn in" the algorithm. Some runs were much longer depending on convergence and stabilization of the resulting posterior distributions.

The model described in this section is an analysis tool and is not intended to characterize the mechanisms by which the different genes are linked. Instead, it is intended to find the most prominent linkages between cells to provide hypotheses that can be further explored and later modeled mechanistically.

Visualization of Gene Networks and Clustering Analysis

We used a MATLAB script newly developed by Parham *et al.* (unpublished data) to generate transcriptional regulatory networks using MATLAB version 6.5 (The MathWorks, Inc., Natick, MA).

Establishment of Mouse *CDK7* Recombinant Retrovirus

A full length cDNA fragment of mouse cyclin-dependent kinase (*Cdk*)*7* (NIH Mammalian Gene bank accession number: NMV009874) was obtained by RT-PCR from the total RNA extracts of 13.5 day mouse embryo using a previously described method [25]. A hemagglutinin (HA) protein tag sequence was then introduced at the carboxyl terminus of this mouse *Cdk7* cDNA using a tailed PCR method. The *Cdk7* cDNA was next subcloned into the EcoRV site of pBluescript SKII+ (Stratagene, La Jolla, CA) by blunt end ligation, and the resulting constructs were validated using a cycle sequencing reaction in an ABI 310 genetic analyzer (Applied Biosystems, Foster City, CA). The subcloned *Cdk7* cDNA fragment was then transferred into the multiple cloning site of an LXIN retrovirus vector (Clontech, Mountain View, CA). Both empty LXIN vector and LXIN vector harboring the mouse *Cdk7* cDNA were introduced into PT67 retrovirus packaging cells (Clontech) using Fugene6 (Roche, Basel, Switzerland). Infected cells were then selected with 1mg/ml G418 (Invitrogen, Carlsbad, CA) in the growth media for one week.

Measurement of the Retrovirus Titers in the Producer Cells

Conditioned medium from the producer cells was diluted 1:10 and 1:50 with DMEM containing 10% calf serum, and then used for the infection of NIH3T3 cells to measure the titer of the synthesized retrovirus. NIH3T3 cells were grown in media with diluted retroviruses for two days under the same conditions that are described below for mouse embryonic fibroblasts. The infected NIH3T3 cells were diluted 1:100 and 1:1000, and then selected with 1mg/ml G418 for one week. Retrovirus titers of the original conditioned medium were calculated based on the number of colonies demonstrating G418 resistance.

Preparation of MEF Cells that Expresses the Recombinant Mouse *CDK7*

Mouse embryonic fibroblasts (MEF) were prepared using a previously described method [25]. Second passage primary fibroblasts at a 70% confluency were infected with conditioned medium containing PT67 producer cells at a 1:2 dilution 1:2 with basal MEF medium for 2 days in the presence of 1μg/ml polybrene (Sigma-Aldrich, St. Louis, MO). When the infected MEF cells reached confluence, they were diluted 1:5 as above and selected with 200μg/ml G418 for one week. Control experiments confirmed that non-infected MEF cells did not survive in the presence of 200μg/ml G418 (data not shown). Infected cells selected with G418 were subjected to lysis and protein extraction for western blot analyses.

Western Blot Analyses of MEF Cells Exogenously Expressing Mouse *CDK7*

Total proteins were isolated from MEF cells infected with either control or Cdk7 recombinant retrovirus using a standard methodology [25]. Heat-denatured proteins were separated by 10% SDS-PAGE and the proteins in the gel were transferred to polyvinylidene difluoride (PVDF) membranes (Immobilon P, Millipore, Billerica, MA). After blocking with 1% non-fat dry milk-Tris buffered saline and 0.1% Tween 20 (TBST), the membranes were probed with anti-HA (High affinity HA 3F10, 1:5,000 dilution, Roche), anti-α-CDK7 (sc-723, 1:5,000 dilution, Santa Cruz, CA), anti-EGFR (kindly provided by Dr. DiAugustine, RP) and anti-N-MYC1 (sc-791, 1:1,000 dilution, Santa Cruz, CA) and anti-c-FOS (sc-52, 1:1,000 dilution, Santa Cruz, CA)antibodies. Blots were then incubated with horseradish peroxidase (HRP)-conjugated rabbit anti-rat IgG (A5795, 1:5,000 dilution, Roche) or donkey anti-rabbit IgG (1:5,000 dilution, GE Healthcare Bioscience) secondary antibodies, respectively. Immunoreactive proteins were detected by enhanced chemiluminescence (P90720, Millipore). Signal intensities from the western blots were detected with X-ray film and quantified using NIH3T3 image software.

RESULTS

Strategy and Analysis of Gene Network Structures

Our experimental strategy is illustrated in Fig. (**1**) and consists of three steps: selection of datasets, visualization and analysis by mathematical modeling, and prediction of biological function through the analysis of transcripts. Genome-wide expression data can provide information linking diverse genes and may be useful as a classification tool to identify alterations in biological processes linked to disease. In contrast, carefully designed analyses of a limited gene group associated with a specific biological process can be used to quantify the dynamics of a gene regulatory network. The genes associated with cell cycle regulation are

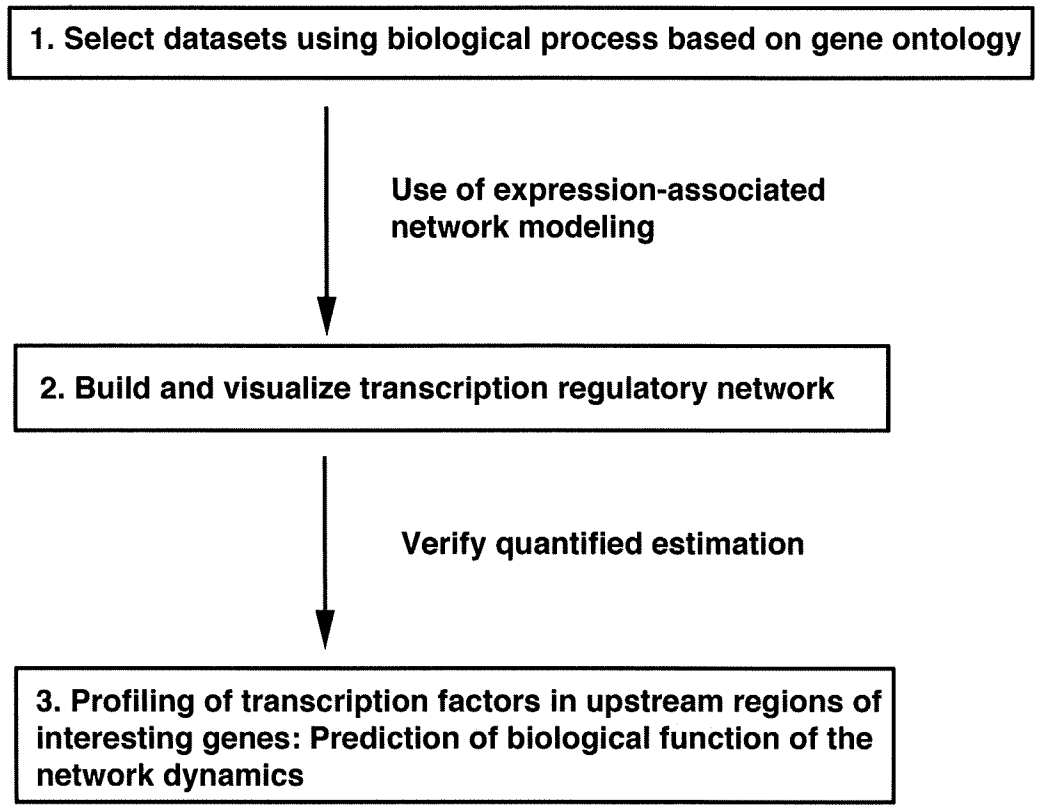

Fig. (1). Strategy used to identify, analyze, and validate regulatory gene networks.

an obvious target for this type of analysis and are the focus of our current study.

The first step in our approach was to select a data subset from a pool of genes associated with various aspects of cell cycle-related processes. The gene choices were based on the gene ontology of the mouse genome using GenMAPP, a computer application designed for the visualization of gene expression data by using maps representing biological pathways. This technique provided a qualitative tool for grouping genes (see Materials and methods). To gather gene expression data associated with the cell cycle, mouse embryo fibroblasts (MEFs) [4] were serum starved or exposed to hydroxyurea to synchronize and control their movement through the cell cycle. At various time points following the release from G0 and cell cycle re-entry, the mRNA expression levels for 6437 genes was measured using a microarray. For 10 cell-cycle related maps (Table **1**), 145 genes were measured in the microarray assay. Of these 145 genes, 50 genes met the criteria of at least 2-fold higher or lower levels as shown in Table **1**. Since the number of genes analyzed using TAO-gen had to be reduced due to computer processing limitations, 39 out of these 50 genes were finally selected for further analysis based on tissue-specific expression information and their biological significance from published articles after removing overlapping genes.

Two separate maps linking our selected 39 genes to a network were generated using the G0 course data subset (serum starvation) and the G1/S course data subset (hydroxyurea treatment). Although the expression of these genes is dynamic during the cell cycle, the networks were modeled by assuming equilibrium between the genes and by evaluating those using formal statistical methods that quantified any linkages and assessed their significance. Nodal genes (genes that appeared to be linked to a large number of other genes) were positively identified in the network. In the final verification step, the promoter regions of the genes targeted by each nodal gene were analyzed for common transcriptional factor binding sites. Finally, we discuss the roles of the central nodes and the dynamics of the quantified network in relation to the murine cell cycle.

Identification of a Gene Network Based on Expression Profiles

Representative maps using our 39 gene networks were developed separately for the G0 course (Fig. **2A**) and the G1/S course (Fig. **3A**). The number of linkages in these two networks is summarized in Table **3**. Name abbreviations of the genes analyzed in this paper are shown according to their listing in GenMAPP. These networks were developed using Bayesian networks and a mathematical model allowing each of these mRNAs to connect to any other through direct or indirect transcriptional regulation leading to gene expression changes.

The network from the G0 course data subset in which the cells had been serum starved indicates that the cyclin-dependent kinase inhibitor 2A (*Cdkn2a*) and *Cdk7* are central nodes (Fig. **2B, C**), whereas *E2f1*, known to regulate the G0-G1 transition, plays a lesser role. Although the *Cdkn2a* and *Cdk7* gene products and related molecules have been suggested to functions in regulating G1 entry and progression from side supportive data [26, 27], it was not clear until our current findings whether these molecules

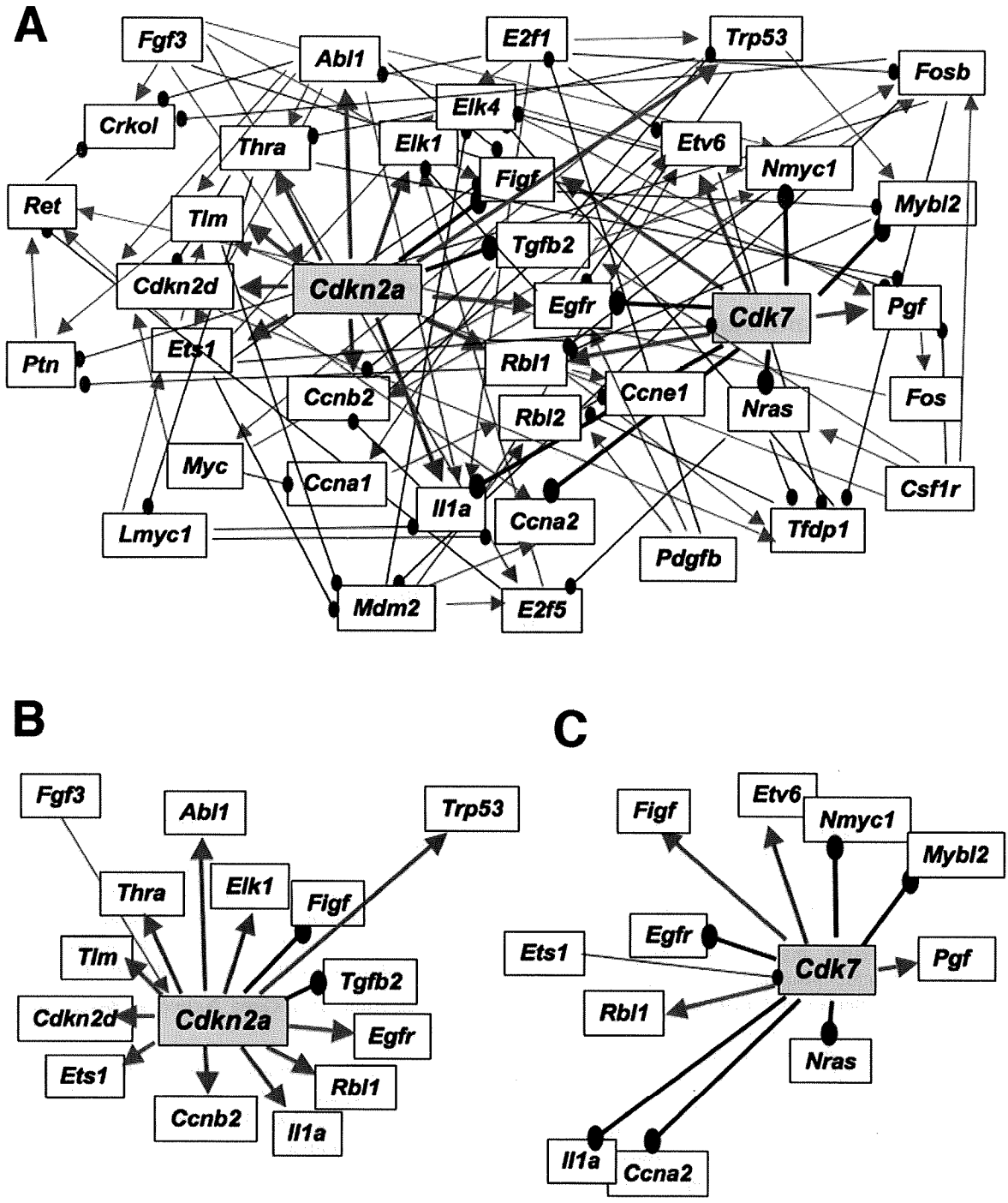

Fig. (2). Representative maps and expression graphs of the transcriptional regulatory networks for selected genes associated with cell-cycle control in MEF cells. Shown are (**A**) the network identified for the G0 course data and also the isolated linkages associated with nodal genes Cdkn2a (**B**) and Cdk7 (**C**). Bold lines indicate linkages from Cdkn2a or Cdk7 as a nodal gene. Red arrows indicate linkages associated with upregulation and blue arrows indicate linkages associated with downregulation for any two genes within the network.

functioned as central nodes in the gene networks. *Cdkn2a* and *Cdk7* were not classified as a G0 cluster *via* k-means in the first report of these microarray data [4]. CDKs are known to be key components of the core cell cycle machinery and are inhibited by cyclin-dependent protein kinase inhibitors (CDKNs). CDK7 and CDKN2A are members of the CDK and CDKN families, respectively. *Cdkn2a* also encodes $p16^{INK4a}$, a protein that indirectly regulates the activities of both pRB and p53 through the inhibition of CDK4 and CDK6. The predictive pathway from *Cdk7* suggests that CDK7 down-regulates *Ccna2*, *Egfr*, *Il1a*, *Mybl2*, *Nmyc1* and *Nras*, and up-regulates *Etv6*, *Figf*, *Pgf* and *Rbl1* (Fig. **2C**). For the time course of the expression levels *of Cdk7, Ccna2, Egfr, Mybl2, N-myc* and *Nras* following the release from serum starvation, when the cells enter G1, the expression levels of *Cdk7* are reduced, resulting in the elevated expression of *Ccna2, Egfr, Mybl2, N-myc and Nras* (data not shown).

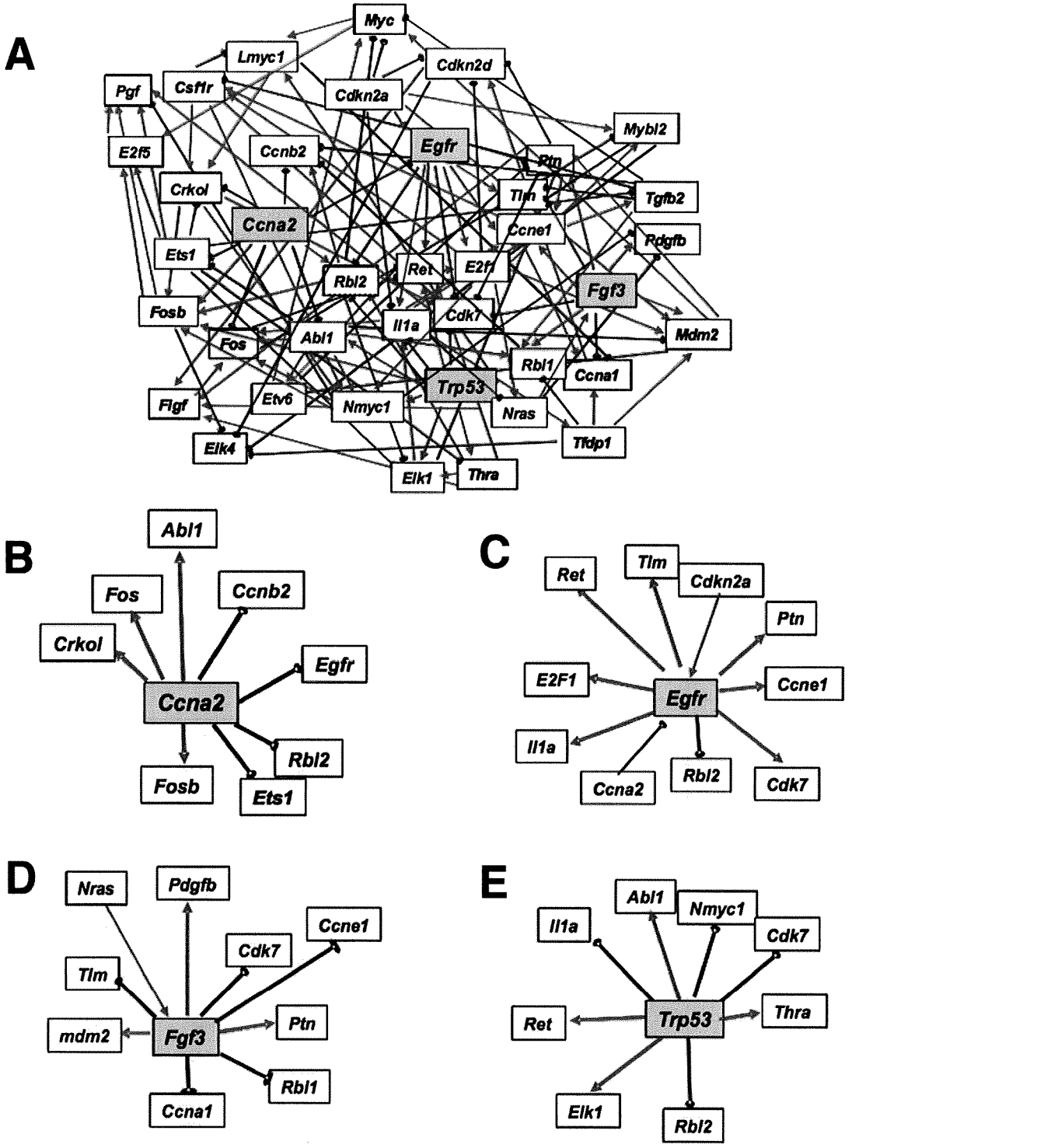

Fig. (3). Networks identified for the G1/S course data (**A**) and the isolated linkages associated with nodal genes Ccna2 (**B**), Egfr (**C**), Fgf3 (**D**) and Trp53 (**E**). Red arrows indicate linkages associated with upregulation and blue arrows indicate linkages associated with downregulation for any two genes within the network. Bold lines indicate linkages with nodal genes.

In the network found for the G1/S start data subset in hydroxyurea treated MEFs, the structure was observed to be more complicated and have no obvious central nodes. In this network, the number of connections from *Cdk7* and *Cdkn2a* to other genes was greatly decreased, whereas the connections from *Ccna2*, *Egfr*, *Fgf3*, *Trp53*, *Nmyc1*, *Ptn*, and *Rbl2* were increased (Fig. **3A**). These changes suggested that growth factors, such as *Egfr*, *Fgf3*, and *Ptn*, and proliferation regulators, such as Ccna2, Trp53, and Rbl2, have more prominent roles during S phase progression (Fig. **3B-E**). From these data, it becomes obvious that the gene networks which regulate the progression of the cell cycle completely differ between the G0-G1 and G1-S transitions.

Table 3. Number of Linkages Between the 39 Selected Genes Related to Cell Cycle Control in MEFs

Gene Name	G0 Course			G1/S Course		
	Outward	Inward	Total	Outward	Inward	Total
Abl1	8	1	9	6	2	8
Ccna1	1	2	3	1	4	5
Ccna2	0	4	4	8	0	8
Ccnb2	2	5	7	0	4	4
Ccne1	0	2	2	3	5	8
Crkol	0	4	4	1	4	5
Csf1r	5	0	5	4	3	7
E2f5	2	3	5	1	3	4
Egfr	4	4	8	8	2	10
Elk1	0	3	3	2	4	6
Elk4	1	5	6	0	4	4
Ets1	6	3	9	6	2	8
Etv6	3	4	7	3	2	5
Fgf3	6	0	6	8	1	9
Figf	1	5	6	1	4	5
Fos	1	1	2	2	5	7
Fosb	5	4	9	3	5	8
Il1a	2	5	7	5	4	9
Lmyc1	3	1	4	2	3	5
Mybl2	1	4	5	2	3	5
Myc	3	1	4	2	5	7
Nmyc1	1	4	5	4	4	8
Nras	2	3	5	5	2	7
Pdgfb	3	0	3	0	3	3
Pgf	1	5	6	0	5	5
Ptn	1	3	4	4	5	9
Ret	1	4	5	0	5	5
Tfdp1	2	5	7	4	1	5
Tgfb2	4	3	7	5	2	7
Thra	3	3	6	4	2	6
Tlm	2	5	7	0	4	4
E2f1	6	0	6	7	3	10
Trp53	4	4	8	8	0	8
Mdm2	4	3	7	3	5	8
Cdkn2a	13	1	14	6	0	6
Cdk7	10	1	11	1	5	6
Rbl1	3	4	7	1	4	5
Rbl2	1	4	5	5	4	9
Cdkn2d	2	4	6	2	4	6

Name abbreviations of the genes analyzed in this study are as listed in Table **2**.

Verification of the Quantified Network

Further analyses were conducted to determine the statistical significance of the linkages between our identified genes. To find the most prominent linkages between genes of the network from Cdk7 and of the network from Trp53, the G0 course dataset and the G1/S course dataset obtained from MEFs treated with serum starvation or hydroxyurea were used, respectively. This analysis method can predict both the strength of the relationships between genes and the posterior distribution of parameters in the log-linear model [22, 23]. Of the 10 genes associated with *Cdk7*, 9 had some posterior densities that did not include 0, suggesting very significant associations (Table **4**). Only Il1a included 0 in the posterior density, with 18% of the distribution above zero and 82% below. This finding suggested a statistically marginal down-regulation. Fig. (**4**) illustrated the distribution for a strong down-regulation (*Cdk7* → *Nras*) and for a weak down-regulation (*Cdk7* → *Il1a*). A negative association between *Nras* and *Cdk7* has been reported previously [28], suggesting that the method we employed in our present analyses can extract negative relationships between two genes using simple microarray data.

Table 4. Summary of the Results from the MCMC Analyses

Parent	Target	Mean	Std.	Percent <0
G0 Network				
Cdk7	Ccna2	-6.0037	0.0718	0
	Egfr	-2.5725	0.0265	0
	Etv6	2.0637	0.0279	0
	Figf	1.4832	0.0022	0
	Il1a	-1.0015	1.0882	17.9
	Mybl2	-2.8674	0.0141	0
	Nmyc1	-0.712	0.0064	0
	Nras	-2.8768	0.0626	0
	Rgf	6.7274	0.0059	0
	Rbl1	1.9701	0.0065	0
G1 Network				
P53	Abl1	0.9456	0.4592	0.0225
	Cdk7	-3.7324	0.0008	0
	Elk1	6.7449	1.3828	0.004
	Il1a	-1.5102	0.0721	0
	Nmyc1	6.1901	0.0417	0
	Rbl1	-6.6934	0.3521	0
	Ret	1.7052	2.7057	25.7

For G0 data, MCMC sampling was performed 140,000 times and the mean, standard deviation (Std.) and percentage below zero were assessed from the last 70,000 samplings. If the number was negative, only the samples above zero were counted. For G1 data, MCMC sampling was performed 300,000 times and the mean, Std., and percentage below zero were assessed from the last 150,000 samplings.

In the G1/S network, *Trp53* suppressed the expression of *Cdk7* and *Rbl2*, and stimulated that of *Abl1*, *Il1a*, *Nmyc*, *Elk1*, *Ret* and *Thra* (Fig. **3E**). *Trp53* has previously been

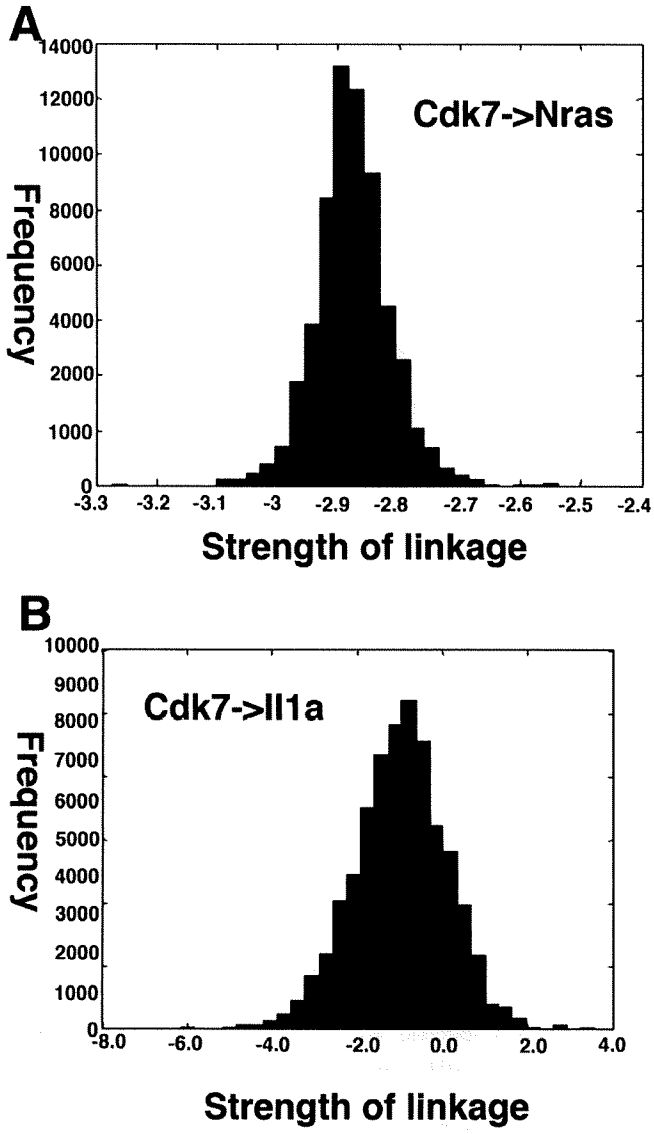

Fig. (4). (**A**, **B**) Frequency histograms approximating the posterior distributions for linkages from Cdk7 to Nras (a statistically significant downregulation) and Cdk7 to Il1a (marginally significant downregulation). Histograms were derived by Bayesian analysis of the gene interaction network shown in Fig. (**2C**) using 70,000 out of 140,000 Markov-Chain Monte Carlo samples and prior distributions as shown in Table **4**.

shown to negatively regulate cyclinD/CDK4, cyclinD/CDK6, cyclinB/cdk2, and cyclinA/cdk2 through the activation of p21 in normal cells. CyclinD/CDK4/6 on the other hand activates phosphorylated RB (pRb) which leads to the activation of E2F, which in turn negatively regulates p53 through $p19^{ARF}$ activation and MDM2 suppression [1, 29]. The interaction between p53 and c-Abl is known to play a critical role in the cell growth and G1 arrest response to DNA damage under normal conditions [30]. It has been reported that CDK7 phosphorylates other CDKs, which is an essential step for their activation [31] and that a direct involvement of p53 in triggering growth arrest by its interaction with the CDK activating kinase complex [32]. These reports and our predictive network suggest therefore that CDK7 is essential for mitosis.

Detection of Gene Networks Using a Recombinant Mouse CDK7 Retrovirus System

Our cell cycle network data indicated that CDK7 activation negatively regulates the expression of *Egfr* and *Nmyc1* in MEFs. To validate this observation, we introduced mouse CDK7 into these cells using a recombinant retrovirus system to evaluate negative regulation of CDK7 against EGFR and N-MYC. The titer of the retrovirus obtained from PT67 producer cells was 4.0 X 10^9 virus copies/ml for the LXIN empty vector and 5.4 X 10^9 virus copies/ml for the CDK7 recombinant retrovirus. The hemagglutinin (HA) protein tag was added to the carboxyl terminus of recombinant CDK7 so that we could distinguish the recombinant protein from its endogenous counterpart.

As shown in Fig. (**5**), western blot detection with a HA antibody revealed the expression of recombinant CDK7 protein in infected MEF cells. Increased levels of total CDK7 protein (endogenous plus recombinant CDK7) was also confirmed by immunoblotting with a CDK7 antibody (Fig. **5A**). The EGFR, N-MYC1 and c-FOS protein levels detected by western blot were decreased in MEF cells infected with the CDK7-expressing retrovirus when compared with the control cells (Fig. **5A**). c-FOS was used as control because there was no direct linkage between CDK7 and c-FOS (see Fig. **2A**). The average levels of EGFR and N-MYC1 from three separate experiments are shown in Fig. (**5B**). Decreased EGFR and N-MYC1 but not c-FOS protein levels indicated that the exogenous introduction of CDK7 negatively influenced their expression. From these results, we concluded that one part of our newly detected cell cycle network had been validated.

DISCUSSION

Gene set enrichment is one means of providing reliable information about specific basic biological processes and has been the most widely used gene-set analysis method to date [33-36]. Directed graphical models known as Bayesian networks, and the MCMC method of determining network inference, have been show to be promising approaches to obtaining new information about gene networks in various tissues and cells.

In our current study, we adopted an approach based on a systematic analysis of gene expression data to define a gene regulatory network and new putative CDK7 functions were identified by quantifying the dynamics of the gene regulatory networks for cell cycle control in MEF cells. A previous study has suggested that a TFIIH complex containing CDK7 is responsible for the phosphorylation of CDK2 and CDK4, both of which are crucial contributors to the G1/S cell cycle transition in human and mouse cells [37]. One of the TFIIH components critically regulates the CAK activity of CDK7 during mitotic progression, suggesting that mitotic silencing of basal transcription is important to the *Drosophila* cell cycle [38]. The previous study indicated that the phosphorylation of CDK7 cause the inhibition of TFIIH-associated kinase and transcriptional activity [39]. Although we do not have any data about the phospholylation status of introduced recombinant CDK7 protein, there is a possibility that the extra amount of CDK7 protein resulted in the reduced transcriptional activity of TFIIH. The gene networks

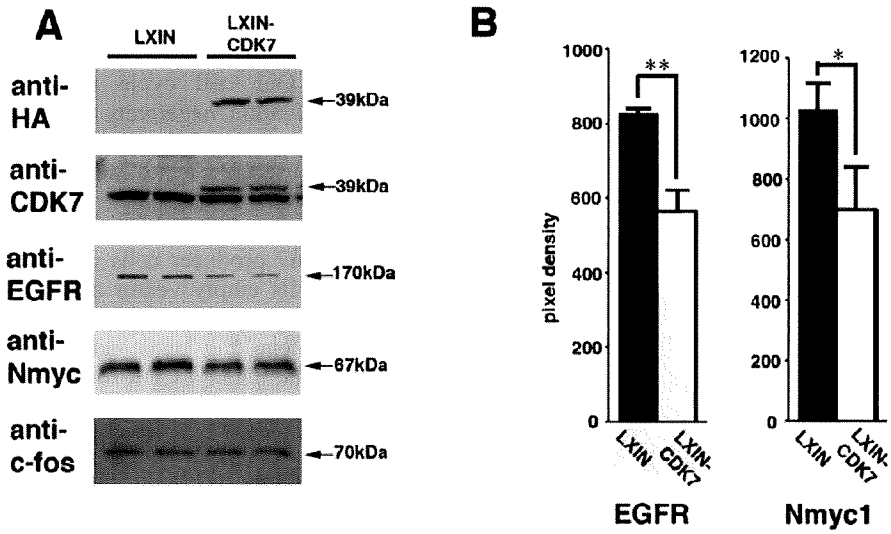

Fig. (5). Experimental verification of detected gene network from Cdk7 to EGFR and N-myc1 using a recombinant retrovirus expression system. (**A**) The protein levels of exogenous Cdk7 (HA), total Cdk7 (Cdk7), EGFR, and N-myc1 were detected by western blotting. Representative blots obtained from two independent samples are shown in the figure. (**B**) EGFR and N-myc1 protein levels were quantitatively analyzed. Data are the average plus standard deviation of 6 western blots from two independent samples for each group. *, $P < 0.05$; **, $P < 0.01$.

found in this study have to be further evaluated in terms of whether they are based on direct or indirect interactions, however, this is to our knowledge the first report showing the importance of CDK7 associated networks for the progression from G0 to G1.

We also analyzed gene networks associated with S phase and M phase, in addition to the progression from G0 to G1, which focused in our current linkage analysis. Several central nodes were detected but their networks will need to be further evaluated experimentally, as shown for CDK7 in this study. We thus reveal that the qualitative algorithm based on Bayesian networks is a useful tool for detecting gene networks that function at specific phases of the cell cycle. Our results indicate that CDK7 negatively regulates EGFR and N-myc expression to control G1 entry. When the MEF cells do enter G1 from G0, the expression of *Cdk7* is suppressed, resulting in the increased expression of the *Egfr and N-myc* genes and protein products. EGFR is known act as a growth factor receptor, and activated EGFR is known to promote cell cycle progression through the G1-related Cyclin complex. N-myc is also known to stimulate cell proliferation and CDK7 thus appears to act as a negative regulator of cell proliferation and cell cycle progression in mammalian cells.

Although the CAK activation at the G1/S phase transition promotes mitotic progression, the relationship between Cdk7 and Egfr was observed at the G0/G1 phase but not the G1/S phase in our case. When we looked for the relationship between two genes at the database GEO (http://www.ncbi.nlm.nih.gov/sites/GDSbrowser) for confirming our data, the relationships are reversal at the early stage after several treatments of serum starvation, cat or Camptothecin. This public evidences can support our data, implicating that CDK7 regulates EGFR expression levels according to the type of cell cycle stage.

Our study detected the gene networks from CDK7 to the downstream. As the next step for the study, these inhibitory effects would be needed to analyze from the viewpoint of kinetics. The kinetics study would explore how fast the transcriptional inhibition reaches to the equilibrium in the process of the cell cycle. The time course analysis with the efficient inducible expression system of recombinant CDK7 would be required to get these data.

Whereas our overall approach in this study was based upon a specific set of tools, other tools could be used to obtain similar findings. Gene ontology was used to select specific genes to consider when defining the network. Other classification methods however, such as clustering, could have also been used to select a specific gene group. Sequence/structure analysis of transcription factors in order to verify gene nodes could be replaced by analyses of protein structure, protein-protein interactions, or protein-DNA interactions. The log-linear mathematical model used to quantify gene interactions could easily be replaced by mechanism-based dynamic models if the data could support more parameters. However, the simplicity of the model used in this analysis has the advantage of providing rapid identification of gene relationships that are helpful in elucidating the structure and dynamics of the gene network using only gene expression profiles. With only one parameter in the model for each gene-gene relationship, one can more easily visualize and understand complex network relationships.

We validated part of our predicted network with a retrovirus CDK7 expression system. The exogenous introduction of mouse CDK7 into MEF cells caused a decrease in the protein levels for EGFR and N-MYC1. These findings provided supporting evidence for the validity of our detected gene network. The molecular weight of the retroviral CDK7 was slightly higher than the endogenous

protein in mouse MEF cells. According to the Genbank database, there is an alternative splice site at the position of exon 6 in CDK7 (accession number: NMV009874.3). Although our cloned CDK7 is the most common form (346aa, 38.9kDa, accession number: NMV009874), and was mainly used in previous functional studies, there is a possibility that endogenous CDK7 expressed in MEF cells is a short form of this protein that arises through the alternative splicing of exon 6. We predict that there is no functional difference between the short form of CDK7 and our recombinant version, since the binding site of MAT7 and phosphorylation sites are present in both forms.

To further test the negative regulatory relationship between CDK7 and EGFR or N-MYC, we attempted to knockdown endogenous CDK7 using a siRNA approach and also a Cre-loxP mediated conditional expression system. However, neither approach was successful in the MEF cells due to a low transfection efficiency for siRNA and the cell toxicity of the adenovirus which expresses the Cre recombinase.

Another important factor to consider is the condition of the MEFs. We used cells that were not immortalized, which allowed us to investigate gene network dynamics in a normal cell context. However, such cells are severely limited in their replicative capacity, resulting in a limited number of applicable approaches for genetic manipulation. Since the inactivation of both p16 and p53 has previously been reported to be essential for the immortalization of MEFs, it is almost certain that the entire cell cycle network would be severely affected by the immortalization process.

An important objective in Bayesian network learning is to infer the network topology. We used 39 genes based on MAP criterion in this study. Even with 39 genes, the topology space is 2^39. However, it is difficult (virtually impossible) to conclude that the optimized network is the best one without doing all possible topologies, an impossibility for 2^{39} topologies. Therefore, a search algorithm, described with step-by-step instructions in the previous work [21], was used to obtain a network topology. Also in the previous work [21], a series of simulation studies were undertaken to address the operating characteristics of the algorithm and to determine the conditions under which it would fail. The analysis used a simple log-linear model to infer linkages in the network. The approach used has advantages and disadvantages over other approaches. The major advantage is a compact parameter space using the minimum number of parameters to infer the network that allows us to use a single parameter to infer the strength of a linkage. This also reflects on the major disadvantage in that is not possible to use this model to describe the dynamics of the interactions *per se* as such a mechanistic model would require more complex biomathematical descriptions of each linkage and considerably more data. That said simple linear models have been a mainstay of descriptive statistical evaluations of biological data for decades. In this case, they allow us to test the hypothesis of no linkage between genes against the alternative of a proportionate change on a log-scale and infer linkage.

The analysis tool used here is able to find genes that appear to be positively or negatively correlated as the gene expression patterns change over time. If a gene is only changed at one time, say 6 hours, and its target genes are only altered at a different time, say 12 hours, this algorithm would be unlikely to identify the linkage. A dynamic model, describing the patterns over time in a more mechanistic fashion, might locate such a linkage, although it might still be very difficult. For the data being examined here, it is more likely that the dynamic changes in gene expression occur gradually throughout the course of the experiment (18-24 hours) resulting in correlations through time that can be observed in our simple linear model.

In summary, the results of our network analyses have raised a number of new possibilities concerning the roles of numerous genes in the regulation of the murine cell cycle. The limitations of these analyses (use of only microarray data, a simple log-linear model, and promoter region sequences) preclude a stronger interpretation of the results. However, as additional data are obtained in future studies that address the hypothetical linkages identified by our findings, it should be possible to bring them formally into an improved analysis and critically evaluate each linkage in greater detail. This is the overall goal of cancer systems biology and the general approach presented here should form the basis for future attempts at system-wide analyses of biological function.

ACKNOWLEDGEMENTS

We thank Leping Li, Delong Liu, Rick Paules, David Umbach, Scott Auerbach and Ben Van Houten (NIH/NIEHS) for their comments on this work, and J. R. Nevins and S. Ishida for kindly providing the original dataset. This research was supported in part by the National Institute of Environmental Health Sciences.

SUPPLEMENTAL MATERIALS

This article also contain supplementary material and it can be viewed at publisher's website along with the article.

REFERENCES

[1] Sears RC, Nevins JR. Signaling networks that link cell proliferation and cell fate. J Biol Chem 2002; 277: 11617-20.

[2] Stillman B. Cell cycle control of DNA replication. Science 1996; 274: 1659-64.

[3] Cho RJ, Huang M, Campbell MJ, *et al.* Transcriptional regulation and function during the human cell cycle. Nat Genet 2001; 27: 48-54.

[4] Ishida S, Huang E, Zuzan H, *et al.* Role for E2F in control of both DNA replication and mitotic functions as revealed from DNA microarray analysis. Mol Cell Biol 2001; 21: 4684-99.

[5] Iyer VR, Eisen MB, Ross DT, *et al.* The transcriptional program in the response of human fibroblasts to serum. Science 1999; 283: 83-7.

[6] Haller F, Gunawan B, von Heydebreck A, *et al.* Prognostic role of E2F1 and members of the CDKN2A network in gastrointestinal stromal tumors. Clin Cancer Res 2005; 11: 6589-97.

[7] Katoh Y, Katoh M. Identification and characterization of DISP3 gene *in silico*. Int J Oncol 2005; 26: 551-6.

[8] Tonon G. From oncogene to network addiction: the new frontier of cancer genomics and therapeutics. Future Oncol 2008; 4: 569-77.

[9] Emmert-Streib F, Dehmer M. Predicting cell cycle regulated genes by causal interactions. PLoS One 2009; 4: e6633.

[10] Margolin AA, Califano A. Theory and limitations of genetic network inference from microarray data. Ann N Y Acad Sci 2007; 1115: 51-72.

[11] Djebbari A and Quackenbush J: Seeded Bayesian Networks: constructing genetic networks from microarray data. BMC Syst Biol 2: 57, 2008.

[12] Gevaert O, De Smet F, Kirk E, *et al.* Predicting the outcome of pregnancies of unknown location: Bayesian networks with expert prior information compared to logistic regression. Hum Reprod 2006; 21: 1824-31.

[13] Nakayama KI, Nakayama K. Ubiquitin ligases: cell-cycle control and cancer. Nat Rev Cancer 2006; 6: 369-81.

[14] Nourse J, Firpo E, Flanagan WM, *et al.* Interleukin-2-mediated elimination of the p27Kip1 cyclin-dependent kinase inhibitor prevented by rapamycin. Nature 1994; 372: 570-3.

[15] Reynisdottir I, Polyak K, Iavarone A, *et al.* Kip/Cip and Ink4 Cdk inhibitors cooperate to induce cell cycle arrest in response to TGF-beta. Genes Dev 1995; 9: 1831-45.

[16] Susaki E, Nakayama K, Nakayama KI. Cyclin D2 translocates p27 out of the nucleus and promotes its degradation at the G0-G1 transition. Mol Cell Biol 2007; 27: 4626-40.

[17] Susaki E, Nakayama KI. Multiple mechanisms for p27(Kip1) translocation and degradation. Cell Cycle 2007; 6: 3015-20.

[18] Tanaka A, Muto S, Konno M, *et al.* A new IkappaB kinase beta inhibitor prevents human breast cancer progression through negative regulation of cell cycle transition. Cancer Res 2006; 66: 419-26.

[19] Matsumoto G, Namekawa J, Muta M, *et al.* Targeting of nuclear factor kappaB Pathways by dehydroxymethylepoxyquinomicin, a novel inhibitor of breast carcinomas: antitumor and antiangiogenic potential *in vivo*. Clin Cancer Res 2005; 11: 1287-93.

[20] Elangovan S, Hsieh TC, Wu JM. Growth inhibition of human MDA-mB-231 breast cancer cells by delta-tocotrienol is associated with loss of cyclin D1/CDK4 expression and accompanying changes in the state of phosphorylation of the retinoblastoma tumor suppressor gene product. Anticancer Res 2008; 28: 2641-7.

[21] Yamanaka T, Toyoshiba H, Sone H, *et al.* The TAO-Gen algorithm for identifying gene interaction networks with application to SOS repair in E. coli. Environ Health Perspect 2004; 112: 1614-21.

[22] Toyoshiba H, Sone H, Yamanaka T, *et al.* Gene interaction network analysis suggests differences between high and low doses of acetaminophen. Toxicol Appl Pharmacol 2006; 215: 306-16.

[23] Toyoshiba H, Yamanaka T, Sone H, *et al.* Gene interaction network suggests dioxin induces a significant linkage between aryl hydrocarbon receptor and retinoic acid receptor beta. Environ Health Perspect 2004; 112: 1217-24.

[24] Dahlquist KD, Salomonis N, Vranizan K, *et al.* GenMAPP, a new tool for viewing and analyzing microarray data on biological pathways. Nat Genet 2002; 31: 19-20.

[25] Fukuda T, Mishina Y, Walker MP, *et al.* Conditional transgenic system for mouse aurora a kinase: degradation by the ubiquitin proteasome pathway controls the level of the transgenic protein. Mol Cell Biol 2005; 25: 5270-81.

[26] Nigg EA. Cyclin-dependent kinase 7: at the cross-roads of transcription, DNA repair and cell cycle control? Curr Opin Cell Biol 1996; 8: 312-7.

[27] Schulze A, Zerfass K, Spitkovsky D, *et al.* Activation of the E2F transcription factor by cyclin D1 is blocked by p16INK4, the product of the putative tumor suppressor gene MTS1. Oncogene 1994; 9: 3475-82.

[28] Abdellatif M, Packer SE, Michael LH, *et al.* A Ras-dependent pathway regulates RNA polymerase II phosphorylation in cardiac myocytes: implications for cardiac hypertrophy. Mol Cell Biol 1998; 18: 6729-36.

[29] Ball KL p21: Structure and Functions Associated with Cyclin-cdk Binding. In: L Meijer, Guidet, S., Philippe, M. (ed.), Progress in cell cycle research: Plenum press, New York, Vol. 3, pp. 125. 1997.

[30] Sionov RV, Coen S, Goldberg Z, *et al.* c-Abl regulates p53 levels under normal and stress conditions by preventing its nuclear export and ubiquitination. Mol Cell Biol 2001; 21: 5869-78.

[31] Larochelle S, Pandur J, Fisher RP, *et al.* Cdk7 is essential for mitosis and for *in vivo* Cdk-activating kinase activity. Genes Dev 1998;12: 370-81.

[32] Schneider E, Montenarh M, Wagner P. Regulation of CAK kinase activity by p53. Oncogene 1998; 17: 2733-41.

[33] Subramanian A, Tamayo P, Mootha VK, *et al.* Gene set enrichment analysis: a knowledge-based approach for interpreting genome-wide expression profiles. Proc Natl Acad Sci U S A 2005; 102: 15545-50.

[34] Goeman JJ, Buhlmann P. Analyzing gene expression data in terms of gene sets: methodological issues. Bioinformatics 2007; 23: 980-7.

[35] Mootha VK, Lindgren CM, Eriksson KF, *et al.* PGC-1alpha-responsive genes involved in oxidative phosphorylation are coordinately downregulated in human diabetes. Nat Genet 2003; 34: 267-73.

[36] Toyoshiba H, Sawada H, Naeshiro I, *et al.* Similar compounds searching system by using the gene expression microarray database. Toxicol Lett 2008.

[37] Watanabe Y, Fujimoto H, Watanabe T, *et al.* Modulation of TFIIH-associated kinase activity by complex formation and its relationship with CTD phosphorylation of RNA polymerase II. Genes Cells 2000; 5: 407-23.

[38] Chen J, Larochelle S, Li X, *et al.* Xpd/Ercc2 regulates CAK activity and mitotic progression. Nature 2003; 424: 228-32.

[39] Akoulitchev S, Reinberg D. The molecular mechanism of mitotic inhibition of TFIIH is mediated by phosphorylation of CDK7. Genes Dev 1998; 12: 3541-50.

Received: May 11, 2009 Revised: February 1, 2010 Accepted: March 1, 2010

Open Access

SUPPLEMENTARY MATERIAL

Importance of CDK7 for G1 Re-Entry into the Mammalian Cell Cycle and Identification of New Downstream Networks Using a Computational Method

Hideko Sone[1,2], Tomokazu Fukuda[3], Hiroyoshi Toyoshiba[1], Takeharu Yamanaka[1], Fred Parham[1] and Christopher J. Portier[1]

[1]*Laboratory of Computational Biology and Risk Analysis, National Institute of Environmental Health Sciences, 111 T.W. Alexander Drive, Research Triangle Park, NC 27709, USA*

[2]*Health Effects Team, National Institute for Environmental Studies, 16-2 Onogawa, Tsukuba 305-8506, Japan*

[3]*Laboratory of Animal breeding and Genetics, Graduate school of Agricultural Science, Tohoku University, Tsutsumidori-amamiyamachi 1-1 Aoba-ku, Sendai 981-8555, Japan*

Supplemental Table 1. Expression Values for Selected 39 Genes for G0-G1

Gene	Time After Serum Starvation (Hours)						
	0	6	12	15	18	21	24
Abl1	9	10	12	12	9	9	23
Ccna1	71	31	39	12	28	21	28
Ccna2	139	144	120	270	402	534	724
Ccnb2	91	44	12	12	9	171	91
Ccne1	137	131	361	637	819	631	606
Crkol	32	11	103	54	44	58	59
Csf1r	42	55	85	53	24	49	38
E2f5	80	35	87	80	68	71	100
Egfr	36	31	15	12	9	9	31
Elk1	14	11	171	227	78	85	187
Elk4	10	61	37	17	9	30	12
Ets1	13	55	38	42	48	19	25
Etv6	33	47	62	65	45	10	52
Fgf3	9	10	19	12	9	9	15
Figf	38	12	124	24	13	23	13
Fos	12	31	12	15	18	22	15
Fosb	13	52	38	13	10	10	13
Il1a	15	33	29	40	27	10	43
Lmyc1	30	46	12	12	67	39	15
Mybl2	102	130	239	302	389	319	405
Myc	142	366	372	430	257	299	251
Nmyc1	12	22	40	15	11	10	58
Nras	11	41	24	15	11	28	31

(Supplemental Table 1) contd.....

Gene	Time After Serum Starvation (Hours)						
	0	6	12	15	18	21	24
Pdgfb	71	52	77	62	19	43	69
Pgf	48	417	64	43	132	181	83
Ptn	446	265	131	223	196	107	124
Ret	50	65	12	36	34	12	14
Tfdp1	77	28	69	164	231	349	187
Tgfb2	84	101	132	26	37	36	46
Thra	79	83	176	168	39	43	118
Tlm	9	24	43	49	26	9	21
E2F1	70	70	72	120	88	100	99
p53	287	511	778	741	538	565	772
mdm2	193	88	98	145	167	207	168
Cdkn2a	9	10	12	12	9	9	15
Cdk7	140	88	102	111	98	111	96
Rbl1	19	11	44	102	109	100	110
Rbl2	76	11	16	20	11	30	35
Cdkn2d	11	11	16	15	58	29	74

Supplemental Table 2. Ratio of Expression Values from 0 Times for Selected 39 Genes for G0-G1

Gene	Time After Serum Starvation (Hours)					
	6	12	15	18	21	24
Abl1	1.11	1.33	1.33	1.00	1.00	2.56
Ccna1	0.44	0.55	0.17	0.39	0.30	0.39
Ccna2	1.04	0.86	1.94	2.89	3.84	5.21
Ccnb2	0.48	0.13	0.13	0.10	1.88	1.00
Ccne1	0.96	2.64	4.65	5.98	4.61	4.42
Crkol	0.34	3.22	1.69	1.38	1.81	1.84
Csf1r	1.31	2.02	1.26	0.57	1.17	0.90
E2f5	0.44	1.09	1.00	0.85	0.89	1.25
Egfr	0.86	0.42	0.33	0.25	0.25	0.86
Elk1	0.79	12.21	16.21	5.57	6.07	13.36
Elk4	6.10	3.70	1.70	0.90	3.00	1.20
Ets1	4.23	2.92	3.23	3.69	1.46	1.92
Etv6	1.42	1.88	1.97	1.36	0.30	1.58
Fgf3	1.11	2.11	1.33	1.00	1.00	1.67
Figf	0.32	3.26	0.63	0.34	0.61	0.34
Fos	2.58	1.00	1.25	1.50	1.83	1.25
Fosb	4.00	2.92	1.00	0.77	0.77	1.00
Il1a	2.20	1.93	2.67	1.80	0.67	2.87
Lmyc1	1.53	0.40	0.40	2.23	1.30	0.50
Mybl2	1.27	2.34	2.96	3.81	3.13	3.97

(Supplemental Table 2) contd.....

Gene	Time After Serum Starvation (Hours)					
	6	12	15	18	21	24
Myc	2.58	2.62	3.03	1.81	2.11	1.77
Nmyc1	1.83	3.33	1.25	0.92	0.83	4.83
Nras	3.73	2.18	1.36	1.00	2.55	2.82
Pdgfb	0.73	1.08	0.87	0.27	0.61	0.97
Pgf	8.69	1.33	0.90	2.75	3.77	1.73
Ptn	0.59	0.29	0.50	0.44	0.24	0.28
Ret	1.30	0.24	0.72	0.68	0.24	0.28
Tfdp1	0.36	0.90	2.13	3.00	4.53	2.43
Tgfb2	1.20	1.57	0.31	0.44	0.43	0.55
Thra	1.05	2.23	2.13	0.49	0.54	1.49
Tlm	2.67	4.78	5.44	2.89	1.00	2.33
E2F1	1.00	1.03	1.71	1.26	1.43	1.41
p53	1.78	2.71	2.58	1.87	1.97	2.69
mdm2	0.46	0.51	0.75	0.87	1.07	0.87
Cdkn2a	1.11	1.33	1.33	1.00	1.00	1.67
Cdk7	0.63	0.73	0.79	0.70	0.79	0.69
Rbl1	0.58	2.32	5.37	5.74	5.26	5.79
Rbl2	0.14	0.21	0.26	0.14	0.39	0.46
Cdkn2d	1.00	1.45	1.36	5.27	2.64	6.73

Supplemental Table 3. Expression Values for Selected 39 Genes for G1-G2

Gene	Time After the Hydroxyl Urea Treatment (Hours)						
	0	3	6	9	12	15	18
Abl1	12	10	9	13	12	15	11
Ccna1	48	39	30	13	42	27	34
Ccna2	488	467	510	447	301	333	526
Ccnb2	12	66	258	189	126	15	27
Ccne1	868	386	274	206	443	534	359
Crkol	67	94	42	95	39	75	36
Csf1r	50	58	85	49	51	91	57
E2f5	40	48	39	58	68	43	31
Egfr	12	10	9	13	12	15	11
Elk1	61	150	17	91	30	73	104
Elk4	11	10	9	38	30	40	10
Ets1	24	33	33	26	70	41	32
Etv6	19	16	30	48	40	49	48
Fgf3	16	10	9	13	12	15	11
Figf	38	17	9	14	11	10	32
Fos	45	57	17	32	77	48	24
Fosb	20	14	14	24	13	13	10

(Supplemental Table 3) contd.....

Gene	Time After the Hydroxyl Urea Treatment (Hours)						
	0	3	6	9	12	15	18
Il1a	44	42	21	23	52	23	35
Lmyc1	66	67	24	84	83	34	43
Mybl2	393	197	245	263	313	293	258
Myc	175	401	188	364	309	219	225
Nmyc1	21	13	13	18	54	23	24
Nras	22	13	11	15	18	16	12
Pdgfb	48	57	60	62	30	66	60
Pgf	46	322	234	197	22	15	11
Ptn	858	520	470	305	448	387	470
Ret	46	12	32	56	11	27	31
Tfdp1	241	249	161	176	233	170	184
Tgfb2	111	62	52	48	53	66	63
Thra	157	114	116	187	147	158	153
Tlm	12	21	26	16	45	63	48
E2F1	200	110	50	82	174	83	97
p53	557	483	455	666	660	627	581
mdm2	373	293	88	125	109	143	72
Cdkn2a	12	10	14	13	12	15	11
Cdk7	59	147	124	76	70	110	90
Rbl1	93	52	49	46	43	100	72
Rbl2	33	23	40	27	18	20	22
Cdkn2d	20	111	74	15	18	16	74

Supplemental Table 4. Ratio of Expression Values from 0 Times for Selected 39 Genes for G1-G2

Genes	Time After the Hydroxyl Urea Treatment (Hours)					
	3	6	9	12	15	18
Abl1	0.83	0.75	1.08	1.00	1.25	0.92
Ccna1	0.81	0.63	0.27	0.88	0.56	0.71
Ccna2	0.96	1.05	0.92	0.62	0.68	1.08
Ccnb2	5.50	21.50	15.75	10.50	1.25	2.25
Ccne1	0.44	0.32	0.24	0.51	0.62	0.41
Crkol	1.40	0.63	1.42	0.58	1.12	0.54
Csf1r	1.16	1.70	0.98	1.02	1.82	1.14
E2f5	1.20	0.98	1.45	1.70	1.08	0.78
Egfr	0.83	0.75	1.08	1.00	1.25	0.92
Elk1	2.46	0.28	1.49	0.49	1.20	1.70
Elk4	0.91	0.82	3.45	2.73	3.64	0.91
Ets1	1.38	1.38	1.08	2.92	1.71	1.33
Etv6	0.84	1.58	2.53	2.11	2.58	2.53
Fgf3	0.63	0.56	0.81	0.75	0.94	0.69

(Supplemental Table 4) contd.....

Genes	Time After the Hydroxyl Urea Treatment (Hours)					
	3	6	9	12	15	18
Figf	0.45	0.24	0.37	0.29	0.26	0.84
Fos	1.27	0.38	0.71	1.71	1.07	0.53
Fosb	0.70	0.70	1.20	0.65	0.65	0.50
Il1a	0.95	0.48	0.52	1.18	0.52	0.80
Lmyc1	1.02	0.36	1.27	1.26	0.52	0.65
Mybl2	0.50	0.62	0.67	0.80	0.75	0.66
Myc	2.29	1.07	2.08	1.77	1.25	1.29
Nmyc1	0.62	0.62	0.86	2.57	1.10	1.14
Nras	0.59	0.50	0.68	0.82	0.73	0.55
Pdgfb	1.19	1.25	1.29	0.63	1.38	1.25
Pgf	7.00	5.09	4.28	0.48	0.33	0.24
Ptn	0.61	0.55	0.36	0.52	0.45	0.55
Ret	0.26	0.70	1.22	0.24	0.59	0.67
Tfdp1	1.03	0.67	0.73	0.97	0.71	0.76
Tgfb2	0.56	0.47	0.43	0.48	0.59	0.57
Thra	0.73	0.74	1.19	0.94	1.01	0.97
Tlm	1.75	2.17	1.33	3.75	5.25	4.00
E2F1	0.55	0.25	0.41	0.87	0.42	0.49
p53	0.87	0.82	1.20	1.18	1.13	1.04
mdm2	0.79	0.24	0.34	0.29	0.38	0.19
Cdkn2a	0.83	1.17	1.08	1.00	1.25	0.92
Cdk7	2.49	2.10	1.29	1.19	1.86	1.53
Rbl1	0.56	0.53	0.49	0.46	1.08	0.77
Rbl2	0.70	1.21	0.82	0.55	0.61	0.67
Cdkn2d	5.55	3.70	0.75	0.90	0.80	3.70

CDK7 ↑ · EGFR ↓

GDS1453

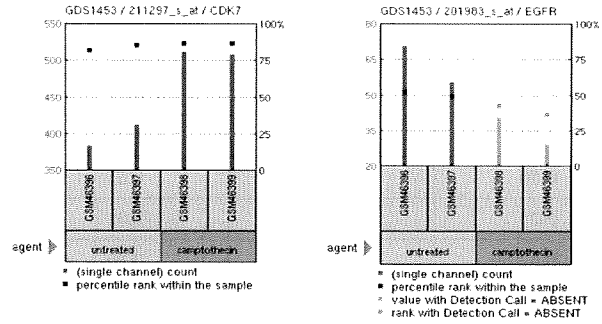

GDS1409

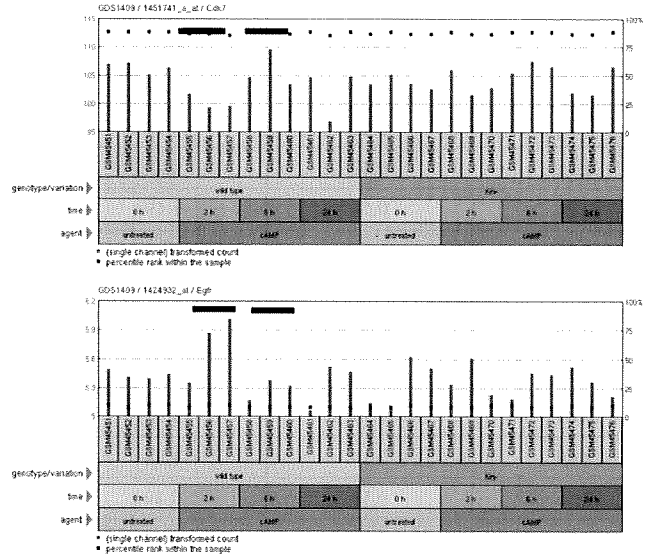

GDS586

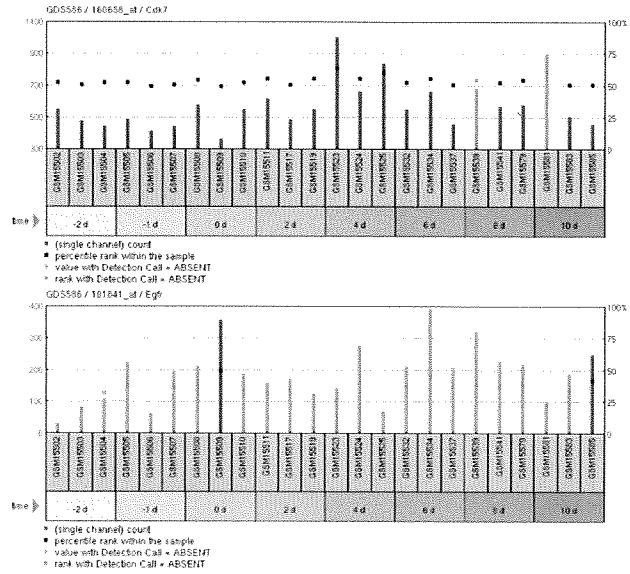

Supplemental Figure. Gene expression profiles for *Cdk7* and *Egfr* extracted from the GEO (http://www.ncbi.nlm.nih.gov/sites/GDSbrowser) studies.

Gene Expression Signatures of Environmental Chemical in Cancer and Developmental Disorders

H Sone[1], S Imanishi[1], A Hiromi[1], G Jia[3], Nagano Reiko[1], T Fukuda[2], S Ohsako[4]

[1]National Institute for Environmental Studies, Tsukuba, Japan; [2]Tohoku University, 1-1 Tsutsumidori-amamiyamachi Aoba-ku, Sendai, 981-8555, Japan, [3]Peking University, Xueyuan Road No 38, Haidian District, Beijing 100191, China; [4]The University of Tokyo, 7-3-1 Bunkyo-ku, Tokyo 113-0033, Japan

Summary

The determination of gene expression signatures as a means to explore cellular responses to chemical exposures offers a new approach for predicting such responses and to investigate chemical agent-gene interactions. Here, we focus on genes responsive to oxidative stress in metal-induced toxicity in rats and humans, and non-metal-induced toxicity in embryonic stem cells. We apply a statistical clustering and a Bayesian network analysis technique, which is a probabilistic graphical model that represents a set of variable identities. We found that the gene expression signature of copper accumulation in the LEC rat liver was unique for this toxic agent. Next, we showed differential gene expression patterns following arsenic exposure in the human liver cell line HepG2 and in human cord blood. Finally, we showed that the gene expression signature of retinoic acid exposure in embryonic stem (ES) cells could be useful for to predicting neuronal disease.

Introduction

The field of molecular genetics has provided a wealth of information regarding the mechanisms underlying environmental chemical (EC)-related carcinogenesis and developmental disorders[1, 2]. Microarray technology has now been used in environmental toxicology studies and has resulted in the establishment of gene expression signatures profiling the toxicity of ECs[3, 4]. Metal ions such as arsenic and copper II induce a variety of oxidative stresses including thiol molecule perturbation, the generation of oxidative DNA adducts and the induction of molecular biomarkers[5-8]. Non-metal chemicals such as the retinoic acids and 2,3,7,8-tetrachlorodebenzo-*p*-dioxin (TCDD) are known to influence oxidative stress-related gene and protein expression during carcinogenesis and in embryonic development[9-12]. Our previous studies have shown that a Bayesian network

technique, which is a probabilistic graphical model that represents a set of variable identities, can be applied to the detection of differences in the gene expression interaction networks that result from exposure to different doses of chemicals[13-16]. Here, we focused on metal-induced toxicity and carcinogenicity, and non-metal-induced toxicity in embryonic stem cells to provide information predicting outcomes, and to better understand the molecular mechanisms underlying these toxicities.

Materials and Methods

We adopted three different approaches in this study: 1) To determine the effects of copper accumulation on oxidative stress marker genes, we performed oligonucleotide array analysis (Affymetrix) in the LEC rat strain (*Atp7b m/m*), which accumulates copper in the liver, and compared the results obtained for LEC rats with those of a sibling line of the *Atp7b w/w* genotype[17-21]. 2) Array data for exposure to arsenic trioxide and other arsenic compounds were obtained from the GEO database (http://www.ncbi.nlm.nih.gov/geo/). For this purpose we performed gene network analysis with data selected from ChemToxGen, which is software that can extract multiple types of information for chemicals. 3) An embryonic stem cell line, B6-G2 (RIKEN), which ubiquitously expresses GFP was exposed to retinoic acids (1 - 100 nM). The differentiation process from embryonic stem to embryonic body formation and neuronal lineage diffretiation was then characterized by gene expression profiling using bead array analysis (Illumina), and the effects of exposure to these compounds were examined. Gene expression signatures of each oxidative stress gene set were established using TAO-Gen (Theoretical algorithm for identifying optimal gene expression networks) Analysis, which is a Bayesian network algorithm (a directed acyclic graph) to describe gene interaction networks

Results and Conclusions

1) Copper-induced gene expression signature. The LEC model showed a unique gene expression profile in which *Npdc1*, *Tradd*, *Med17*, *Psmd1*, *Insig11*, *Abcc2*, and *G6pc* were differentially expressed in the copper-exposed LEC liver compared to wild-type siblings (Table 1). Expression of these genes was significantly increased or decreased in comparison with the expression of known oxidative stress-responsive genes. To establish whether copper-induced signatures in this model were unique, 40 GEO datasets with in the search term Affymetrix GeneChip Rat Expression Set (GPL341) were scrutinized (http://www.ncbi.nlm.nih.gov/sites/entrez) and subjected to hierarchical clustering analysis (Fig. 1). Within these 40 datasets, four clusters similar

to the LEC liver signature were identified, namely "Lung response to cigarette smoke (GDS2194)", "High Fe/low Fe at 12 weeks (GDS1027, GDS1054, GDS2073)", "Aged marrow-derived stromal cell response to dexamethasone (GDS1280, GDS2231)" and "Liver response to skin burn (GDS1273, 964, 1393, 1959, 2237)". This analysis suggested that gene expression signatures resulting from copper accumulation in the LEC rat liver were infrequent, although similar patterns could be detected under certain other stress conditions. The combination of the 7 genes identified here may be useful biomarkers for oxidative stress-related cancer.

2) Heavy metals in the Public Database. We further analyzed arsenic-induced gene expression profiles in order to compare them with the gene expression signature of copper exposure. Networks of oxidative stress-related genes were classified according to chemical exposure dosage and also by the types of arsenic used in different experiments. Array datasets (GDS2780 and GSE7967) for heavy metals were obtained from the GEO database (http://www.ncbi.nlm.nih.gov/geo/). To predict common biomarkers and understand molecular mechanisms, we performed gene network analysis with Bayesian algorithms on liver carcinoma HepG2 cells exposed to different heavy metals in the GDS 2780 study and on human cord blood exposed to arsenic at different concentrations in the GSE7967 study. The results provide insight into the molecular basis of heavy metal cytotoxicity in the HepG2 study. In the GSE7967 study, the gene expression pattern suggested activation of Inflammation and NFκB signaling in infants born to arsenic-exposed mothers. Cord blood was collected at birth from infants whose mothers were exposed or unexposed to arsenic (0.1 - 68.63 mg/g) in the study. Therefore, we divided the subjects into 4 groups according to blood as concentrations (0.1, 1.76, 9.66, 68.63 mg/g). Expression array data are shown for the MAP kinase pathway, which is an important inflammation pathway (Fig. 2). Eleven oxidative stress-related genes were then selected and analyzed in two groups (mean blood concentration 0.142 μg/g in the low exposure group and 21.41 μg/g in the high exposure group) by the Bayesian network algorithm. The results of this analysis showed that *GSS* and *PRDX* regulate *TRDD*, *NUDT1*, *SOD1* and *INSIG1* in the low exposure group, and that *NUD1* regulates *TRDD*, *TXNRD2* and *PRDX2* in the high exposure group, suggesting that anti-oxidative stress-related genes play a key role in to protection against cellular damage in the low exposure group, but a DNA damage-related gene is dominant in the high exposure group, in which cell damage would progress.

3) *Retinoic acid-induced gene expression profiles reflecting developmental differentiation and disease*. In the early stage of neuronal development, the ES to EB

neuronal lineages differentiation period, it is known that exposure to RA activates anti-oxidative stress systems. Oxidative stress-responsive genes play roles in neuronal differentiation and development of disease such as Alzheimer's disease. Therefore, we analyzed gene signatures during neuronal development. Gene expression profiling and gene-network analysis, in terms of oxidative stress-related genes, revealed different signatures during neuronal lineage differentiation induced by retinoic acids. For the neuronal disease-related gene set including oxidative stress-responsive genes (Table 2), the gene-interaction network indicated that ubiquitination was activated and apoptosis was inhibited due to exposure to RA. This was despite the finding that the Sod system was activated with copper from App and ApoE and apoptosis was promoted under control conditions in differentiated neuronal cells (Fig. 4). Our current approaches could thus provide a useful way to obtain information on the properties of specific hazardous chemicals. Gene expression profiling and gene-network analysis revealed signatures for retinoic acid treatment in terms of oxidative stress-related genes, suggesting that they play different roles in early embryonic toxicity.

In conclusion, Gene expression signatures for oxidative stress associated with copper accumulation in the rat liver, heavy metals and RA exposure in mouse embryonic stem cells could effectively facilitate biomarker discovery and the improved understanding of molecular mechanisms of environmental chemical effects on cancer and developmental disorders.[22]

Table 1. List of genes changed remarkably in the LEC rat liver

Gene Name	Fold change*	Annotation, Function
Npdc1	12.1	Neural proliferation, differentiation and control,1
Tradd	11.5	TNFRSF1A-associated via death
Med17	10.5	Mediator complex subunit 17
Psmd1	8.8	Proteasome 26S subunit, non-ATPase, 1
Insig1	-7.7	Insulin induced gene 1
Abcc2	-6.2	ATP-binding cassette, sub-family C (CFTR/MRP), member 2
G6pc	-6.1	Glucose-6-phosphatase, catalytic

*Values were confirmed by semi-quantitative RT-PCR